

# JAGN1 deficiency causes aberrant myeloid cell homeostasis and congenital neutropenia

Kaan Boztug<sup>1,2</sup>, Päivi M Järvinen<sup>3</sup>, Elisabeth Salzer<sup>1</sup>, Tomas Racek<sup>3</sup>, Sebastian Mönch<sup>3</sup>, Wojciech Garncarz<sup>1</sup>, E Michael Gertz<sup>4</sup>, Alejandro A Schäffer<sup>4</sup>, Aristotelis Antonopoulos<sup>5</sup>, Stuart M Haslam<sup>5</sup>, Lena Schieck<sup>6</sup>, Jacek Puchalka<sup>3</sup>, Jana Diestelhorst<sup>3,6</sup>, Giridharan Appaswamy<sup>6</sup>, Brigitte Lescoeur<sup>7</sup>, Roberto Giambruno<sup>1</sup>, Johannes W Bigenzahn<sup>1</sup>, Ulrich Elling<sup>8</sup>, Dietmar Pfeifer<sup>9</sup>, Cecilia Domínguez Conde<sup>1</sup>, Michael H Albert<sup>3</sup>, Karl Welte<sup>6</sup>, Gudrun Brandes<sup>10</sup>, Roya Sherkat<sup>11</sup>, Jutte van der Werff ten Bosch<sup>12</sup>, Nima Rezaei<sup>13</sup>, Amos Etzioni<sup>14</sup>, Christine Bellanné-Chantelot<sup>15</sup>, Giulio Superti-Furga<sup>1</sup>, Josef M Penninger<sup>8</sup>, Keiryn L Bennett<sup>1</sup>, Julia von Blume<sup>16</sup>, Anne Dell<sup>5</sup>, Jean Donadieu<sup>17</sup> & Christoph Klein<sup>3</sup>

**The analysis of individuals with severe congenital neutropenia (SCN) may shed light on the delicate balance of factors controlling the differentiation, maintenance and decay of neutrophils. We identify 9 distinct homozygous mutations in the *JAGN1* gene encoding Jagunal homolog 1 in 14 individuals with SCN. *JAGN1*-mutant granulocytes are characterized by ultrastructural defects, a paucity of granules, aberrant N-glycosylation of multiple proteins and increased incidence of apoptosis. *JAGN1* participates in the secretory pathway and is required for granulocyte colony-stimulating factor receptor-mediated signaling. *JAGN1* emerges as a factor that is necessary in the differentiation and survival of neutrophils.**

SCN, first described by Rolf Kostmann<sup>1</sup>, is characterized by life-threatening bacterial infections caused by a paucity of mature neutrophils. Studies of individuals with SCN have highlighted principles governing the differentiation, homeostasis and functions of neutrophils<sup>2</sup>, illustrated by roles for *ELANE*<sup>3,4</sup> and *G6PC3* (ref. 5) in endoplasmic reticulum (ER) stress or *HAX1* in mitochondrial function<sup>6</sup>. Genetic defects affecting the endosomal-lysosomal system have been associated with congenital neutropenia (*AP3B1* (ref. 7), *LAMTOR2* (ref. 8), *VPS13B*<sup>9</sup> and *VPS45* (refs. 10,11)); other genes mutated in monogenic SCN include *GFI1* (ref. 12) and *WAS*<sup>13</sup>.

We herein report that *JAGN1* is an ER-resident protein with a function in the early secretory pathway and is critical for the differentiation and maintenance of human neutrophils.

We studied two sibships of Algerian origin (family A; Fig. 1a) that originated from the same Sephardic community and shared a family name. Consanguinity could not be proven, but several familial links were found. Five children in family A had SCN associated with recurrent, severe bacterial infections (Table 1). Histological analysis of bone marrow smears showed maturation arrest at the promyelocyte/myelocyte stage (Supplementary Fig. 1). Sequencing of *ELANE*, *HAX1* and *G6PC3* yielded no mutations.

We performed a SNP array-based genetic linkage analysis as described previously<sup>14</sup>, identifying a single perfectly segregating interval between 9.52 Mb and 11.04 Mb on chromosome 3 of Build 36.3 of the NCBI human genome (Fig. 1a) that contained 30 genes (Supplementary Table 1). The interval had a multi-marker logarithm of odds (LOD) score of at least 4.5, with a score of at least 6.0 if the sibships were assumed to have a common ancestor (Online Methods).

We performed a literature search to prioritize genes in the linkage interval (Supplementary Table 1) for Sanger sequencing. Because aberrant ER function had previously been documented in individuals with mutations in *ELANE*<sup>3,4</sup> and *G6PC3* (refs. 5,15), *JAGN1*—encoding an ER-resident protein originally characterized in *Drosophila melanogaster*<sup>16</sup>—was an attractive candidate. Sanger sequencing identified one homozygous mutation that segregated perfectly with the disease in both sibships of family A. This mutation, c.3G>A in exon 1 of the *JAGN1* gene, leads to disruption of the defined start site of translation (Supplementary Fig. 2). For confirmatory evidence, exome sequencing of subject P2 was performed. *JAGN1* was the sole

<sup>1</sup>CeMM Research Center for Molecular Medicine of the Austrian Academy of Sciences, Vienna, Austria. <sup>2</sup>Department of Pediatrics and Adolescent Medicine, Medical University of Vienna, Vienna, Austria. <sup>3</sup>Department of Pediatrics, Dr. von Hauner Children's Hospital, Ludwig Maximilians University, Munich, Germany. <sup>4</sup>Computational Biology Branch, National Center for Biotechnology Information, US National Institutes of Health, Bethesda, Maryland, USA. <sup>5</sup>Department of Life Sciences, Imperial College London, London, UK. <sup>6</sup>Department of Pediatric Hematology/Oncology, Hannover Medical School, Hannover, Germany. <sup>7</sup>Department of Hematology, Hospital R Debré, Paris, France. <sup>8</sup>Institute of Molecular Biotechnology of the Austrian Academy of Sciences (IMBA), Vienna, Austria. <sup>9</sup>Department of Hematology, Oncology and Stem Cell Transplantation, University Medical Center Freiburg, Freiburg, Germany. <sup>10</sup>Department of Cell Biology, Hannover Medical School, Hannover, Germany. <sup>11</sup>Acquired Immunodeficiency Research Center, Isfahan University of Medical Sciences, Isfahan, Iran. <sup>12</sup>Department of Pediatrics, Hospital of the Free University of Brussels, Brussels, Belgium. <sup>13</sup>Research Center for Immunodeficiencies, Pediatrics Center of Excellence, Children's Medical Center, Tehran University of Medical Sciences, Tehran, Iran. <sup>14</sup>Division of Pediatrics and Immunology, Rappaport School of Medicine, Technion, Haifa, Israel. <sup>15</sup>Genetics Department, AP-HP Pitié-Salpêtrière Hospital, Pierre and Marie Curie University, Paris, France. <sup>16</sup>Max Planck Institute of Biochemistry, Martinsried, Germany. <sup>17</sup>Neutropenia Registry, Reference Center for Hereditary Immunodeficiencies, Pediatric Hematology, AP-HP, Armand Trousseau Children's Hospital, Paris, France. Correspondence should be addressed to C.K. ([christoph.klein@med.uni-muenchen.de](mailto:christoph.klein@med.uni-muenchen.de)).

Received 26 January; accepted 25 July; published online 17 August 2014; doi:10.1038/ng.3069

**Figure 1** Identification of mutations in *JAGN1*. (a) Genotypes of affected (filled symbols) and unaffected (open symbols) individuals from family A on chromosome 3p. (b) Exon-intron diagram of the *JAGN1* gene locus with the positions of all alterations identified in this study. (c) *JAGN1* protein expression was determined by immunoblot analysis using an antibody directed against the N-terminal end of *JAGN1*, as outlined in the Online Methods. PX denotes subject number X in this study, and PXF denotes the respective father; HD, healthy donor.

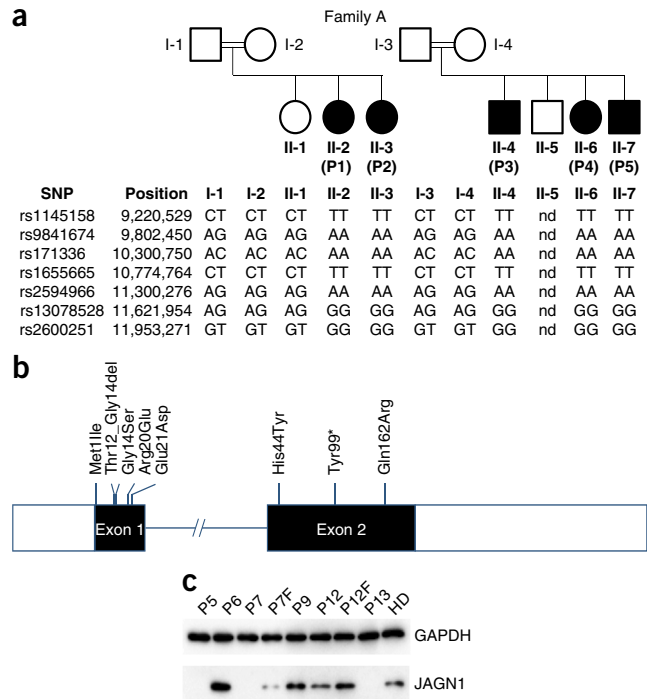
gene in **Supplementary Table 1** having a variant meeting our filtering criteria (Online Methods and **Supplementary Table 2**).

Thereafter, we assessed a cohort of 74 individuals with SCN for mutations in *JAGN1* and identified 9 additional individuals from 8 families bearing homozygous mutations in this gene (**Fig. 1b** and **Table 1**). The majority of the variants were missense mutations; however, one subject had a nonsense mutation (**Fig. 1b**, **Table 1**, **Supplementary Fig. 3** and **Supplementary Table 3**). Immunoblot analysis on subject-derived Epstein-Barr virus (EBV)-immortalized B cell lines using antibodies recognizing the N terminus of *JAGN1* showed that different mutations resulted in decreased or non-detectable protein levels in some subjects (P5, P7 and P13) and expression of a mutant and likely non-functional protein in others (P9 and P12) (**Fig. 1c**). Immunoblot analysis in subject-derived fibroblast cell lines confirmed the findings for P12 and P13 and showed that the non-frameshift deletion mutation in P14 led to decreased expression of a *JAGN1* protein variant of slightly reduced molecular weight (**Supplementary Fig. 4**).

In the clinical findings (**Table 1**), there was not an obvious distinction between individuals with SCN with *JAGN1* mutations and those with *ELANE* mutations<sup>17</sup> or *HAX1* mutations<sup>6</sup> of the non-syndromic type, but we occasionally observed abnormalities in bone, pancreas or teeth (**Table 1**). Serial blood counts from several subjects did not show a genotype-phenotype relationship (**Supplementary Table 4**). Overall, variability in the level of neutropenia cannot easily be associated with the distinct genotypes. For instance, all affected individuals in family A had the same mutation but exhibited different disease severities. This variability is reminiscent of SCN with *ELANE*<sup>18</sup> or *G6PC3* (refs. 5,19) mutations where no clear association between genotype and phenotype has been observed, suggesting that modifier genes or environmental factors might influence neutrophil counts. Heterozygous *JAGN1* mutation carriers were found to have normal differential blood counts (data not shown). Interestingly, the response to recombinant human granulocyte colony-stimulating factor (rhG-CSF) treatment was poor in several *JAGN1*-deficient individuals (**Supplementary Table 4**), and, in some individuals, severe bone pain limited the use of rhG-CSF.

*JAGN1* orchestrates the concentration of the ER into subcortical clusters during the vitellogenesis stage of *Drosophila* oogenesis<sup>16</sup>. We performed transmission electron microscopy studies to assess the ultrastructure of the ER and granules in neutrophils. In contrast to the ER in healthy myeloid progenitor cells, the ER in *JAGN1*-mutant cells appeared enlarged and granules were almost completely absent (**Fig. 2a**). Comparison by transmission electron microscopy of peripheral blood neutrophils isolated from a healthy donor before injection with rhG-CSF to those isolated the day after injection did not identify marked differences in the ultrastructure of the cells (**Supplementary Fig. 5**), suggesting that G-CSF treatment is not primarily responsible for the altered ultrastructure observed in *JAGN1*-deficient myeloid cells. Consistent with the observation of increased ER stress, the protein levels of binding immunoglobulin protein (BIP; encoded by the *HSPA5* gene) were elevated in *JAGN1*-mutant granulocytes (**Fig. 2b**).

In light of the differences observed in ER structure in *JAGN1*-mutant granulocytes, we performed comparative global glycomic



analyses of peripheral blood neutrophils. The N-glycomes of neutrophils from the clinically healthy mother (**Fig. 2c**) and father (**Supplementary Fig. 6**) resembled the N-glycomes of healthy control samples analyzed in earlier studies<sup>20,21</sup>. We treated an unrelated healthy donor with rhG-CSF 1 d before neutrophil isolation and analyzed the N-glycosylation pattern. No qualitative changes in N-glycan content or in the abundance of multi-fucosylated N-glycan structures were detected (**Supplementary Fig. 7**). In contrast to the healthy donor neutrophils with intact *JAGN1*, *JAGN1*-mutant neutrophils from subjects P7 and P8 exhibited anomalous N-glycomic profiles, characterized by a marked reduction in the fucosylation of all multiantennary glycans (**Fig. 2c** and **Supplementary Fig. 8**). Although immature N-glycans were similar in abundance to the ones in healthy control samples (**Supplementary Fig. 6**), their high-mass N-glycomes showed a decrease in the abundance of fucosylated antennae (**Fig. 2c**). Studies on unrelated subjects P3 and P12 gave similar findings, with even more pronounced defects (**Supplementary Fig. 9**). In contrast to N-glycan structures, O-glycosylation patterns were similar in cells from affected subjects and controls (**Supplementary Fig. 10**).

Because defective expression of neutrophil elastase (ELANE) has been implicated in the pathomechanism of SCN<sup>22,23</sup>, we assessed whether *JAGN1* had an effect on the expression, glycosylation or localization of ELANE. We analyzed ELANE protein expression by immunoblot and determined its subcellular localization using immunofluorescence in cells in which *JAGN1* had been knocked down using small interfering RNAs (siRNAs). No difference in either expression or subcellular localization was seen (**Supplementary Fig. 11**). Furthermore, the N-glycosylation profile of ELANE did not depend on *JAGN1*, as documented by the treatment of cellular extracts with peptide N-glycosylase (PNGase) and endoglycosidase H (EndoH) (**Supplementary Fig. 11**).

We assessed whether *JAGN1* deficiency was associated with increased incidence of apoptosis in neutrophils, as seen in individuals with mutations in *ELANE*<sup>3,4</sup>, *HAX1* (ref. 6) or *G6PC3* (ref. 5). Peripheral blood neutrophils were exposed to the protein kinase

**Table 1 Clinical and molecular characteristics of individuals with SCN**

Individual	Sex	Country of origin (consanguinity)	ANCs (per $\mu$ l) before G-CSF therapy	Bone marrow smear (before G-CSF therapy)	ANCs (per $\mu$ l) at recent follow-up	JAGN1 genotype (homozygous) and protein alteration	Infections	Extrahematopoietic symptoms	Age and status in mid-2013
P1 (AII-2)	F	Algeria (consanguinity suggested)	830	Maturation arrest	370	c.3G>A; p.Met11Ile	ENT infections, aphthosis, perianal cellulitis, skin abscesses	None	23 years; alive and well
P2 (AII-3)	F	Algeria (consanguinity suggested)	800	No maturation arrest	800	c.3G>A; p.Met11Ile	ENT infections	Short stature (height of 1.46 m)	17 years; alive and well
P3 (AII-4)	M	Algeria (consanguinity suggested)	570	Maturation arrest (intermittent)	430	c.3G>A; p.Met11Ile	Aphthosis, skin abscesses, balanitis, pneumonitis, lung abscess, osteitis perianal cellulitis	Pyloric stenosis	19 years; alive and well
P4 (AII-6)	F	Algeria (consanguinity suggested)	501	Maturation arrest (intermittent)	270	c.3G>A; p.Met11Ile	Otitis, paraodontopathy	Scoliosis, dental malformations	17 years; alive and well
P5 (AII-7)	M	Algeria (consanguinity suggested)	165	Maturation arrest	230	c.3G>A; p.Met11Ile	ENT infections, aphthosis, skin abscesses, pneumonitis, lung abscess, perianal cellulitis	None	5 years; alive and well
P6 (BII-1)	F	Iran (consanguineous)	892	Maturation arrest	501	c.59G>A; p.Arg20Glu	Upper respiratory tract infections, pneumonia, skin abscesses	Febrile convulsion, focal epilepsy	12; alive and well
P7 (CII-1)	M	Turkey (consanguineous)	191	Maturation arrest	819	c.130C>T; p.His44Tyr	Upper respiratory tract infections, pneumonia, skin and perianal abscesses, sepsis ( <i>Haemophilus influenza</i> )	Extramedullary hematopoiesis with thickening of skull bones	10 years; alive and well
P8 (CII-2)	F	Turkey (consanguineous)	Missing	Maturation arrest	3,587	c.130C>T; p.His44Tyr	Upper respiratory tract infections, skin abscess	Bilateral hip dysplasia, extramedullary hematopoiesis with thickening of skull bones	7 years; alive and well
P9 (DII-1)	F	Iran (consanguineous)	920	Maturation arrest	1,479	c.40G>A; p.Gly14Ser	Skin abscesses, onycholysis	None	28; alive and well
P10 (EII-1)	M	Israel (consanguineous)	130	Maturation arrest	n/a	c.297C>G; p.Tyr99*	Aspergillosis (none after HSCT)	Severe osteoporosis and repeated bone fractures (continuing after HSCT)	13 years; HSCT at the age of 9 months due to therapy-refractory neutropenia, alive and well
P11 (FII-1)	F	Morocco (consanguineous)	70	Maturation arrest (intermittent)	563	c.485A>G; p.Gln162Arg	Skin abscesses, omphalitis, pancolitis	Lipomatosis, pancreatic insufficiency, bone abnormalities, dental malformations	Died at age 5 years owing to pancolitis and septicemia
P12 (GII-1)	F	Albania (consanguineous)	408	Maturation arrest	555	c.63G>T; p.Glu21Asp	Upper respiratory tract infections, pneumonia, skin abscess	Short stature (5 cm below third percentile), amelogenesis imperfecta, neurodevelopmental delay	16 years; alive and well
P13 (HII-3)	F	Pakistan (no known consanguinity)	290	Maturation arrest, slight dyserythropoiesis	1,491	c.485A>G; p.Gln162Arg	ENT infections, upper respiratory tract infections, pneumonia, sepsis ( <i>Escherichia coli</i> )	Failure to thrive (height 5 cm below third percentile, weight 3.8 kg below third percentile), coarctation of the aorta, mild developmental delay	0 years; alive, awaiting HSCT
P14 (III-1)	F	Germany (no known consanguinity)	128	Maturation arrest	n/a	c.35_43del CCGACGGCA; p.Thr12_Gly14del	Pneumonia (none after HSCT), bronchiectasis	None	25 years; G-CSF non-responder, HSCT at age 20 years due to secondary acute myeloid leukemia, alive and well

For the two families included in the linkage analysis (see also Fig. 1), consanguinity was suggested as they belong to the same ancestry subgroup and originate from the same village. ENT, ear, nose and throat; ANC, absolute neutrophil count; HSCT, hematopoietic stem cell transplant; M, male; F, female.

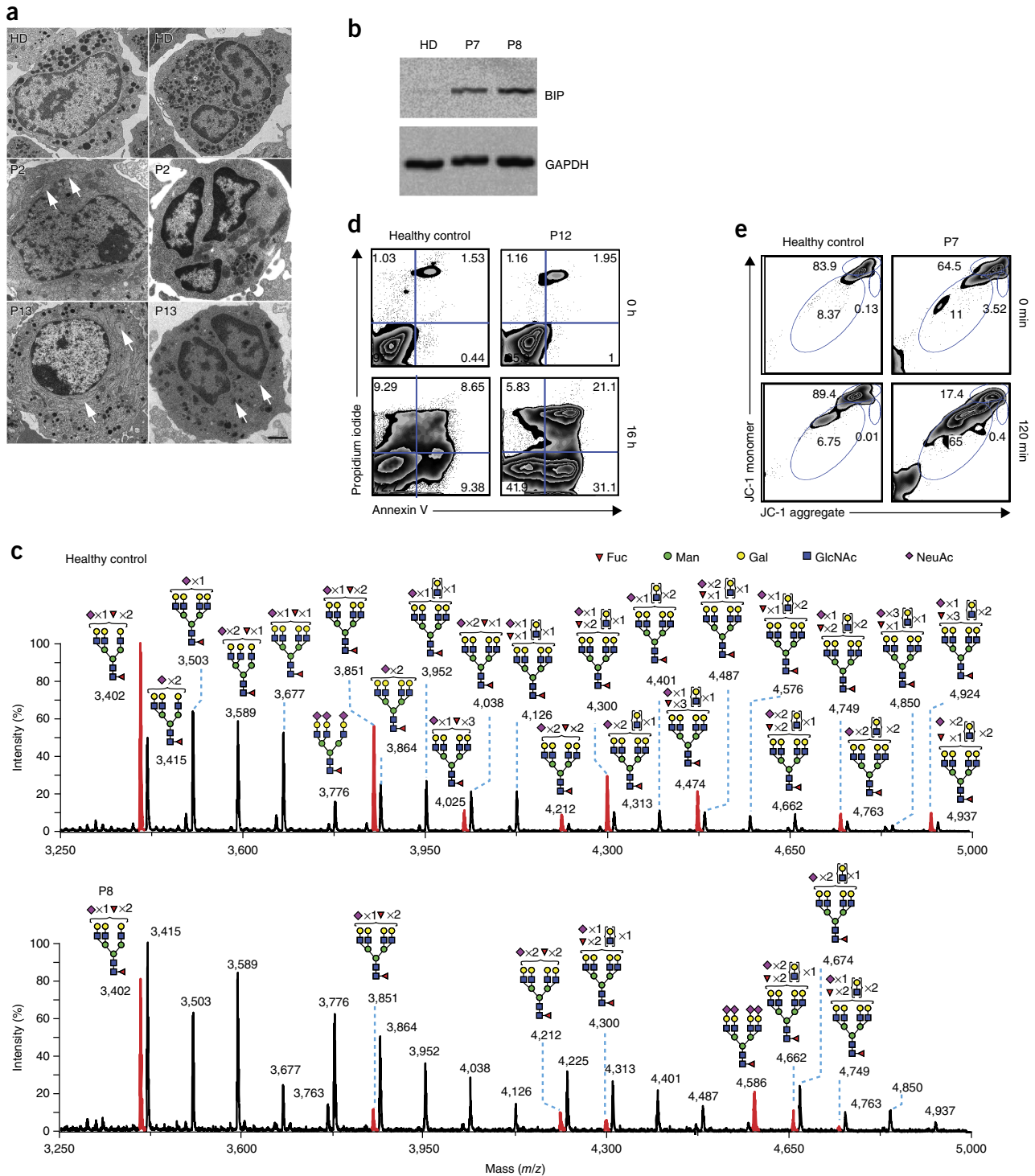


**Figure 2** Phenotype of *JAGN1*-mutant neutrophils. **(a)** Transmission electron microscopy of the bone marrow. Myelocytes (left) from affected subjects showed aberrant, enlarged ER structures (arrows) in contrast to myelocytes from a healthy donor (HD). Differentiated granulocytes (right) from affected subjects showed a paucity of typical granules (arrows). Scale bar, 1  $\mu$ m. **(b)** Increased protein expression of BIP in *JAGN1*-mutated granulocytes from subjects P7 and P8. **(c)** Matrix-assisted laser desorption ionization time-of-flight (MALDI-TOF) mass spectrometry partial spectra of the permethylated N-glycans isolated from a heterozygous carrier (healthy control; mother from family C) and subject P8 with a *JAGN1* mutation. The structures detected at mass-per-charge ( $m/z$ ) ratios of 3,402, 3,851, 4,212, 4,300 and 4,749 were found in reduced abundance in affected subjects in comparison to healthy controls, whereas those detected with  $m/z$  ratios of 4,025, 4,474 and 4,924 in healthy controls were almost undetectable in affected subjects. Red peaks represent glycans whose abundance is markedly altered in the affected subject. For clarity, black peaks in the spectrum for the affected subject are not annotated. See the top panel for annotations. Structure assignments are based on composition, tandem mass spectrometry and biosynthetic knowledge. Fuc, fucose; Man, mannose; Gal, galactose; GlcNAc, N-acetylglucosamine; NeuAc, N-acetylneuraminic acid. **(d)** Increased incidence of apoptosis in *JAGN1*-mutant neutrophils (P12) in response to staurosporine, as determined by flow cytometry analysis using Annexin V and propidium iodide. **(e)** *JAGN1*-mutated neutrophils (P7) show rapid loss of mitochondrial membrane potential ( $\Delta\psi_{m}$ ) upon stimulation with valinomycin, as determined by flow cytometry analysis using the lipophilic cation JC-1 as a dye.

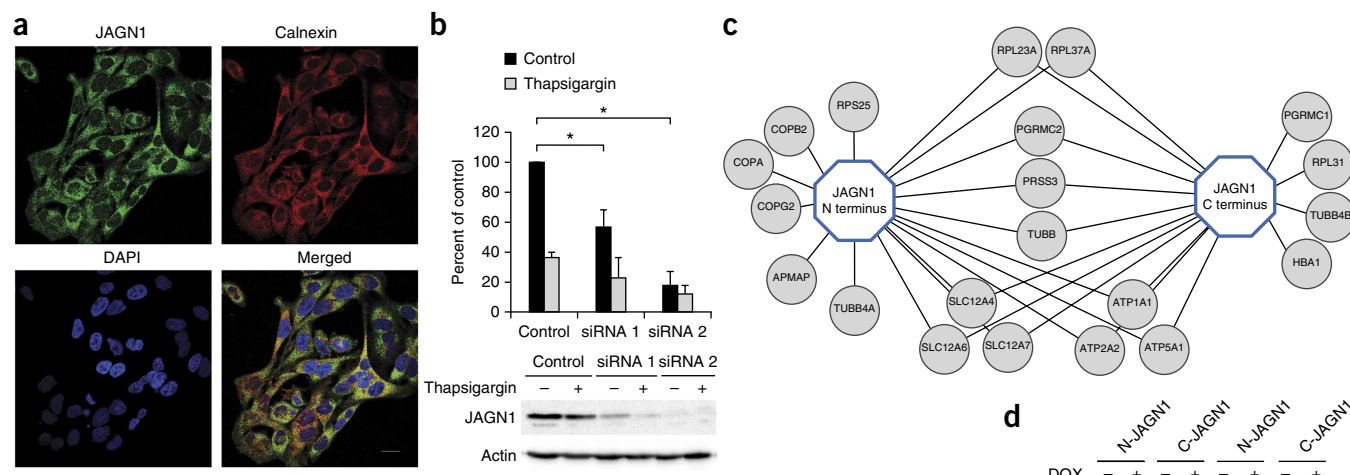


**Figure 3** A role for JAGN1 in the secretory pathway. **(a)** Endogenous JAGN1 colocalizes mainly with the ER protein calnexin. HeLa cells were stained with antibodies to JAGN1 (green) and calnexin (red), for visualization of the ER. DAPI staining (4',6-diamidino-2-phenylindole; blue) was used to visualize nuclei. Images were acquired with a confocal laser scanning microscope fitted with a 63 $\times$  objective. Scale bar, 20  $\mu$ m. **(b)** siRNA-mediated knockdown of *JAGN1* leads to significantly decreased secretion of *Gaussia* luciferase in comparison to control siRNA. Scrambled siRNA was used as the control. Thapsigargin was used as a positive control for secretion, as it induces ER stress. Results are shown as the ratio between samples averaged over three independent experiments. Statistical significance was calculated using a two-tailed Student's *t* test; \**P* < 0.05. Error bars, s.d. **(c)** Determination of the JAGN1 protein complex. Tandem affinity purification of STREP-HA-tagged N- and C-terminal JAGN1 protein complexes followed by liquid chromatography mass spectrometry identified several interacting proteins, including members of the COPI complex. **(d)** Immunoprecipitation of COPA and COPB2 using STREP-HA-tagged N- and C-terminal JAGN1 was performed and confirmed physical interaction between these proteins, consistent with the data in **c**. IP, immunoprecipitation; DOX, doxycycline. **(e)** Immunoblotting to study the glycosylation pattern of G-CSF-R in neutrophils from affected subjects. Neutrophils were isolated from the blood of a healthy donor and from the affected subjects of three families (P13, P2 and P12). Neutrophils from the healthy donor were also treated with PNGase F to remove glycans. GAPDH served as a loading control in **d** and **e**.

inhibitor staurosporine, which induces ER stress and can lead to apoptosis. A higher percentage of JAGN1-deficient neutrophils underwent apoptosis in comparison to neutrophils from healthy individuals (Fig. 2d and Supplementary Fig. 12). To assess whether the intrinsic pathway of apoptosis was involved, we treated neutrophils with valinomycin, a potassium-specific transporter that causes dissipation of the mitochondrial membrane potential ( $\Delta\psi_{mt}$ ). JAGN1-deficient neutrophils had a propensity to rapidly depolarize  $\Delta\psi_{mt}$  (Fig. 2e and Supplementary Fig. 13).

Next, we determined the subcellular localization of JAGN1 in mammalian cells. Using a JAGN1-specific polyclonal antibody, we found that JAGN1 was predominantly localized to the ER in HeLa cells (Fig. 3a). This localization was confirmed in immunofluorescence microscopy studies using constructs encoding GFP-fused JAGN1 in fibroblasts and HeLa cells (Supplementary Fig. 14).

We sought to determine whether JAGN1 deficiency affected the secretory pathway. We measured the secretion of *Gaussia* luciferase in HeLa cells in which *JAGN1* expression was reduced by RNA-mediated interference. In cells with siRNA-mediated knockdown of *JAGN1*, the secretion of *Gaussia* luciferase was significantly reduced (Fig. 3b). The secretion of proteins, however, was not globally affected; cells with *JAGN1* knockdown were not different from controls with respect to the secretion of horseradish peroxidase (HRP; data not shown).

As it was unknown why JAGN1 might be necessary for the secretory pathway, we performed affinity purification followed by mass spectrometry to identify the interaction partners of JAGN1. N- and C-terminal JAGN1 streptavidin-binding peptide-hemagglutinin (STREP-HA) constructs were generated in HEK293T cells, and tandem affinity purifications were performed as previously described<sup>24</sup>. Three

members of the coat protein I (COPI) complex (COPA, COPB2 and COPG2) were identified as interacting with JAGN1 (Fig. 3c and Supplementary Data Set 1). Coimmunoprecipitation experiments confirmed the interactions for both COPA and COPB2 (Fig. 3d). The COPI complex is known to have a central role in vesicular trafficking from the Golgi complex to the ER<sup>25</sup>.

From clinical trials of rhG-CSF, it is known that 5–10% of both congenital and acquired neutropenia cases respond poorly to rhG-CSF<sup>26</sup>, but no predictive biomarker or molecular mechanism has been found. The majority of individuals deficient for JAGN1 showed no or poor therapeutic response to rhG-CSF. The cognate receptor for G-CSF, G-CSF-R, is heavily glycosylated<sup>27</sup> and is relevant for the development of neutrophils<sup>28</sup>. Global assessment of glycosylation (Fig. 2c and Supplementary Figs. 6–10) implicated a defect in N-glycosylation in neutrophils from affected subjects. We hypothesized that inadequate G-CSF-R-mediated signaling might offer an explanation for the observed defects in neutrophil differentiation. In comparison to neutrophils isolated from healthy individuals, JAGN1-deficient neutrophils derived from affected subjects displayed decreased abundance of G-CSF-R, which was of reduced molecular weight (Fig. 3e). Upon treatment of proteins with PNGase F, no difference in molecular weight could be demonstrated, suggesting that a defect in N-glycosylation accounts for the aberrant molecular weight of G-CSF-R in affected individuals (Fig. 3e). It remains difficult to determine the relative contributions of aberrant G-CSF-R signaling and increased apoptosis to neutropenia.

We attempted to model JAGN1 deficiency using siRNA-mediated knockdown of *JAGN1* in HeLa cells. However, HeLa cells did not recapitulate increased ER stress upon *JAGN1* knockdown

(Supplementary Fig. 15a) or easily detectable differences in G-CSF-R N-glycosylation (Supplementary Fig. 15b), indicating that there might be cell type-specific differences between primary neutrophils and HeLa cells. Knockdown of *JAGN1* did not have any influence on the pattern of subcellular G-CSF-R distribution (Supplementary Fig. 15c). Next, we expressed G-CSF-R in HeLa cells and studied STAT3 phosphorylation upon exposure to rhG-CSF in cells transfected with *JAGN1*-specific siRNA, as suggested by previous research on G-CSF signaling<sup>29</sup>. In contrast to cells transfected with control siRNA, HeLa cells with *JAGN1* knockdown had reduced phosphorylation of STAT3 upon exposure to rhG-CSF (Supplementary Fig. 15d). Collectively, these data suggest decreased G-CSF-R-dependent signaling in the absence of *JAGN1*. Because of discrepancies between HeLa cells and primary neutrophils, we cannot prove precise molecular mechanisms.

Using transmission electron microscopy, biochemical studies and analysis of the N-glycome, we show that *JAGN1*-deficiency is associated with alterations in the ER and specific granules in human neutrophils. Additionally, *JAGN1* deficiency is associated with aberrant neutrophil N-glycosylation. Most striking is a substantial reduction in antennae fucosylation (Fig. 2c and Supplementary Fig. 8).

Other human monogenic diseases have both SCN and aberrant membrane trafficking. Mutations in *AP3B1*, encoding the  $\beta$  subunit of the adaptor protein 3 (AP3) complex that is involved in protein sorting in the lysosomal compartment and related organelles, are the cause of Hermansky-Pudlak syndrome type II, a syndromic disorder including congenital neutropenia<sup>7,30</sup>. Reduced expression of the endosomal adaptor protein p14/LAMTOR2 causes a congenital neutropenia syndrome associated with aberrant lysosomal function and defective G-CSF-R signaling<sup>8</sup>. Cohen syndrome is caused by mutations in *VPS13B*<sup>9</sup>, which encodes a peripheral Golgi membrane protein with a critical function in maintaining the integrity of the Golgi ribbon<sup>31</sup>. The SEC1P/MUNC18-like protein VPS45, cycling on and off membranes during vesicle transport in yeast<sup>32</sup>, is essential for SNARE-mediated membrane trafficking<sup>33</sup>. *VPS45* mutations have been identified in individuals with SCN with extramedullary hematopoiesis, suggesting that the encoded protein contributes to the viability and migration of neutrophils<sup>10,11</sup>. All diseases mentioned in this paragraph are recessive.

Even though *JAGN1* is ubiquitously expressed, the only phenotype of *JAGN1* deficiency seen in all affected subjects was congenital neutropenia. This cell type specificity could either occur because some other protein carries out the function of *JAGN1* in other cell types (as G6PC1 can replace G6PC3, but not in hematopoietic cells<sup>5</sup>) or because *JAGN1* is essential for the secretion and/or membrane localization of proteins necessary for neutrophil function. In line with the latter hypothesis, we could demonstrate aberrant expression of G-CSF-R, a critical cytokine receptor governing the differentiation of neutrophils.

In an accompanying report, Wirnsberger *et al.* confirm the relevance of *Jagn1* for neutrophil granulocytes in a mouse knockout model<sup>34</sup>. Even though, in contrast to humans with *JAGN1* mutations, *Jagn1*-deficient mice do not show neutropenia, they are characterized by increased susceptibility to fungal infections owing to the defective killing capacity of neutrophil granulocytes. Interestingly, granulocyte/macrophage colony-stimulating factor (GM-CSF) but not G-CSF rescues this functional defect in mice<sup>34</sup>, potentially opening a new therapeutic option for individuals with *JAGN1*-deficient SCN. In summary, by identifying individuals with *JAGN1* deficiency, we define a role for *JAGN1* in the early secretory pathway that is required for the physiological differentiation and viability of neutrophils.

## METHODS

Methods and any associated references are available in the [online version of the paper](#).

*Note: Any Supplementary Information and Source Data files are available in the online version of the paper.*

## ACKNOWLEDGMENTS

The authors thank the patients and their families for their participation in this study. The help of all contributing medical, technical and administrative staff is greatly appreciated. The authors thank J. Colinge for bioinformatics analysis of the mass spectrometry data. The authors thank G. Leverger, H. Ducou Lepointe, J. Levin, the association IRIS (Immunodéficience Primitive, Recherche, Information, Soutien) and V. Grosjean for their support. This study was supported by CeMM intramural funds and the FWF (Austrian Science Fund) START Programme (to K.B.) and by grants from the European Research Council (Advanced Grants to C.K. and J.P.; Starting Grant to K.B.), the European Program on Rare Diseases (E-RARE Neuro-Net) and the German Research Foundation (SFB914 and Gottfried-Wilhelm-Leibniz Program). The work at Imperial College was supported by the Biotechnology and Biological Sciences Research Council (BBSRC; grants BB/F0083091 and BB/K016164/1). The French SCN registry is supported by grants from Amgen, Chugai, Fondation Maladies Rares, the Institut de Veille Sanitaire, INSERM, the Association Sportive de Saint Quentin Fallavier, CEREDIH (Reference Center for Hereditary Immunodeficiencies) and the Société d'Hémo-Immunologie Pédiatrique. This research is supported in part by the Intramural Research Program of the US National Institutes of Health, the National Library of Medicine, the DZIF (German Center for Infection Research) and the Care-for-Rare Foundation.

## AUTHOR CONTRIBUTIONS

K.B. identified the *JAGN1* mutation in the index family and the majority of the other families reported and performed experiments together with P.M.J., E.S., S.M., W.G., L.S., J. Diestelhorst, G.A., J.v.B. B.L., M.H.A., K.W., R.S., J.v.d.W.t.B., N.R., A.E., J. Donadieu, C.B.-C. and C.K. took care of and enrolled patients into the study. T.R., E.M.G., A.A.S., J.P. and D.P. were responsible for genome-wide analyses and bioinformatics analysis. A.A., S.M.H. and A.D. performed glycoprotein analysis. G.B. performed transmission electron microscopy analyses. E.S., R.G., J.W.B., C.D.C., G.S.-F. and K.L.B. performed *JAGN1* interactome experiments and data analysis. U.E. and J.M.P. generated and characterized the polyclonal antibodies and gave critical advice. C.K. designed and coordinated the investigations. The manuscript was written by C.K. and K.B. with help from E.M.G., A.A.S. and P.M.J. The final version of the manuscript was approved by all authors.

## COMPETING FINANCIAL INTERESTS

The authors declare no competing financial interests.

Reprints and permissions information is available online at <http://www.nature.com/reprints/index.html>.

- Kostmann, R. Infantile genetic agranulocytosis; agranulocytosis infantilis hereditaria. *Acta Paediatr. Suppl.* **45** (suppl. 105), 1–78 (1956).
- Klein, C. Genetic defects in severe congenital neutropenia: emerging insights into life and death of human neutrophil granulocytes. *Annu. Rev. Immunol.* **29**, 399–413 (2011).
- Grenda, D.S. *et al.* Mutations of the *ELA2* gene found in patients with severe congenital neutropenia induce the unfolded protein response and cellular apoptosis. *Blood* **110**, 4179–4187 (2007).
- Köllner, I. *et al.* Mutations in neutrophil elastase causing congenital neutropenia lead to cytoplasmic protein accumulation and induction of the unfolded protein response. *Blood* **108**, 493–500 (2006).
- Boztug, K. *et al.* A syndrome with congenital neutropenia and mutations in *G6PC3*. *N. Engl. J. Med.* **360**, 32–43 (2009).
- Klein, C. *et al.* HAX1 deficiency causes autosomal recessive severe congenital neutropenia (Kostmann disease). *Nat. Genet.* **39**, 86–92 (2007).
- Dell'Angelica, E.C., Shotelersuk, V., Aguilar, R.C., Gahl, W.A. & Bonifacio, J.S. Altered trafficking of lysosomal proteins in Hermansky-Pudlak syndrome due to mutations in the  $\beta$ 3A subunit of the AP-3 adaptor. *Mol. Cell* **3**, 11–21 (1999).
- Bohn, G. *et al.* A novel human primary immunodeficiency syndrome caused by deficiency of the endosomal adaptor protein p14. *Nat. Med.* **13**, 38–45 (2007).
- Kolehmainen, J. *et al.* Cohen syndrome is caused by mutations in a novel gene, *COH1*, encoding a transmembrane protein with a presumed role in vesicle-mediated sorting and intracellular protein transport. *Am. J. Hum. Genet.* **72**, 1359–1369 (2003).
- Stepensky, P. *et al.* The Thr224Asn mutation in the *VPS45* gene is associated with congenital neutropenia and primary myelofibrosis of infancy. *Blood* **121**, 5078–5087 (2013).

11. Vilboux, T. *et al.* A congenital neutrophil defect syndrome associated with mutations in *VPS45*. *N. Engl. J. Med.* **369**, 54–65 (2013).
12. Person, R.E. *et al.* Mutations in proto-oncogene *GF11* cause human neutropenia and target *ELA2*. *Nat. Genet.* **34**, 308–312 (2003).
13. Devriendt, K. *et al.* Constitutively activating mutation in WASP causes X-linked severe congenital neutropenia. *Nat. Genet.* **27**, 313–317 (2001).
14. Glocker, E.-O. *et al.* A homozygous *CARD9* mutation in a family with susceptibility to fungal infections. *N. Engl. J. Med.* **361**, 1727–1735 (2009).
15. Jun, H.S. *et al.* Lack of glucose recycling between endoplasmic reticulum and cytoplasm underlies cellular dysfunction in glucose-6-phosphatase- $\beta$ -deficient neutrophils in a congenital neutropenia syndrome. *Blood* **116**, 2783–2792 (2010).
16. Lee, S. & Cooley, L. Jagunal is required for reorganizing the endoplasmic reticulum during *Drosophila* oogenesis. *J. Cell Biol.* **176**, 941–952 (2007).
17. Dale, D.C. *et al.* Mutations in the gene encoding neutrophil elastase in congenital and cyclic neutropenia. *Blood* **96**, 2317–2322 (2000).
18. Horwitz, M.S. *et al.* Neutrophil elastase in cyclic and severe congenital neutropenia. *Blood* **109**, 1817–1824 (2007).
19. Boztug, K. *et al.* Extended spectrum of human glucose-6-phosphatase catalytic subunit 3 deficiency: novel genotypes and phenotypic variability in severe congenital neutropenia. *J. Pediatr.* **160**, 679–683 (2012).
20. Babu, P. *et al.* Structural characterisation of neutrophil glycans by ultra sensitive mass spectrometric glycomics methodology. *Glycoconj. J.* **26**, 975–986 (2009).
21. Hayee, B. *et al.* *G6PC3* mutations are associated with a major defect of glycosylation: a novel mechanism for neutrophil dysfunction. *Glycobiology* **21**, 914–924 (2011).
22. Horwitz, M.S., Corey, S.J., Grimes, H.L. & Tidwell, T. *ELANE* mutations in cyclic and severe congenital neutropenia: genetics and pathophysiology. *Hematol. Oncol. Clin. North Am.* **27**, 19–41 (2013).
23. Tidwell, T. *et al.* Neutropenia-associated *ELANE* mutations disrupting translation initiation produce novel neutrophil elastase isoforms. *Blood* **123**, 562–569 (2014).
24. Rudashevskaya, E.L. *et al.* A method to resolve the composition of heterogeneous affinity-purified protein complexes assembled around a common protein by chemical cross-linking, gel electrophoresis and mass spectrometry. *Nat. Protoc.* **8**, 75–97 (2013).
25. Duden, R. ER-to-Golgi transport: COP I and COP II function. *Mol. Membr. Biol.* **20**, 197–207 (2003).
26. Dale, D.C. *et al.* A randomized controlled phase III trial of recombinant human granulocyte colony-stimulating factor (filgrastim) for treatment of severe chronic neutropenia. *Blood* **81**, 2496–2502 (1993).
27. Li, J. & Sartorelli, A.C. Evidence for the glycosylation of the granulocyte colony-stimulating factor receptor. *Biochem. Biophys. Res. Commun.* **205**, 238–244 (1994).
28. Welte, K., Zeidler, C. & Dale, D.C. Severe congenital neutropenia. *Semin. Hematol.* **43**, 189–195 (2006).
29. de Koning, J.P. *et al.* The membrane-distal cytoplasmic region of human granulocyte colony-stimulating factor receptor is required for STAT3 but not STAT1 homodimer formation. *Blood* **87**, 1335–1342 (1996).
30. Jung, J. *et al.* Identification of a homozygous deletion in the *AP3B1* gene causing Hermansky-Pudlak syndrome, type 2. *Blood* **108**, 362–369 (2006).
31. Seifert, W. *et al.* Cohen syndrome-associated protein, COH1, is a novel, giant Golgi matrix protein required for Golgi integrity. *J. Biol. Chem.* **286**, 37665–37675 (2011).
32. Bryant, N.J. & James, D.E. The Sec1p/Munc18 (SM) protein, Vps45p, cycles on and off membranes during vesicle transport. *J. Cell Biol.* **161**, 691–696 (2003).
33. Carpp, L.N., Ciuffo, L.F., Shanks, S.G., Boyd, A. & Bryant, N.J. The Sec1p/Munc18 protein Vps45p binds its cognate SNARE proteins via two distinct modes. *J. Cell Biol.* **173**, 927–936 (2006).
34. Wirnsberger, G. *et al.* Jagunal homolog 1 is a critical regulator of neutrophil function in fungal host defense. *Nat. Genet.* doi:10.1038/ng.3070 (17 August 2014).

## ONLINE METHODS

**Subjects.** All material from affected individuals and healthy donors was obtained with informed assent/consent in accordance with the Declaration of Helsinki. The study was approved by the institutional review boards at Hannover Medical School and the Ludwig Maximilians University Munich.

**Genome-wide genetic linkage analysis.** For family A, DNA samples from five affected individuals, four parents and one unaffected sibling were genotyped using the Affymetrix 250k StyI SNP mapping array (Gene Expression Omnibus (GEO) platform [GPL3718](#)), following the procedures in ref. 35 and those recommended by Affymetrix.

Genotypes were analyzed using the software *findhomoz*<sup>14</sup> to identify intervals where the affected individuals were homozygous for the same genotypes at consecutive markers and the unaffected individuals had different genotypes for some markers in the interval. The same or a similar homozygosity mapping procedure was used for families B–G to identify an interval on 3p consistent with linkage that included *JAGN1*. For families E and F, we used another Affymetrix chip (GEO platform [GPL6801](#)) for genotyping.

For family A, we computed LOD scores using the software Superlink<sup>36</sup> for some of the 257 SNPs in a 3-Mb region on chromosome 3 that included the minimal linkage region and >500 kb of additional sequence on each side. Twenty of the 257 SNPs had perfect and fully informative segregation.

To model likely consanguinity in pedigrees, we added hypothetical ancestors to the two nuclear family pedigrees. The parents on the left (I-1 and I-2) were assumed to have a pair of great grandparents in common, and the parents on the right (I-3 and I-4) were assumed to have a different pair of great grandparents in common. First, the pedigrees were kept separate and the LOD scores were summed over the two pedigrees. In a model of the unproven shared ancestry of the carrier parents, one great grandparent on the left was assumed to share a pair of great grandparents with a great grandparent on the right, such that the putative founder pair was six generations before the carrier parents. The assumption of common great grandparents to represent likely consanguinity has been used previously<sup>12,37</sup>.

Disease was modeled as fully penetrant recessive with a disease allele frequency of 0.001. LOD scores depended on the frequency of the disease-associated marker alleles. After identifying the 20 SNPs that segregated perfectly, we chose 7 SNPs (**Fig. 1a**) at which to compute single-marker LOD scores and obtained their affected allele frequencies from HapMap<sup>38</sup>. These seven SNPs were selected as described below such that no two had extreme linkage disequilibrium. The affected allele frequency of each SNP was taken to be the largest (leading to the lowest possible LOD score) frequency among the four populations in HapMap. The multipoint LOD scores reported in the results were computed using the seven selected SNPs.

HapMap Phase 2 had linkage disequilibrium data for four populations (CEU, Utah residents of European ancestry; YRI, Yoruba from Nigeria; JPT, Japanese from Tokyo; CHB, Chinese from Beijing). We considered two SNPs to be in 'extreme linkage disequilibrium' with each other if HapMap explicitly listed an  $r^2$  value of at least 0.8 between the SNPs in any of the four populations or if there was a third SNP with which we considered the first and second SNPs to be in extreme linkage disequilibrium. This means that if there was a chain of SNPs with  $r^2$  values of at least 0.8 connecting the first and second SNP, where each  $r^2$  value is the maximum for the four populations, that the SNPs were considered to be in extreme linkage disequilibrium.

**Exome sequencing.** Exome sequencing of subject P2 was performed using 50 ng of genomic DNA. DNA was fragmented with simultaneous adaptor ligation (tagmentation) using the Nextera transposome. Subsequently, adaptor-ligated genomic DNA was enriched for exonic regions during PCR amplification. Clusters were generated using the Illumina cBot Cluster Generation System, following the TruSeq PE Cluster Kit v3 Reagent Preparation Guide. Sequencing was performed in a multiplexed pool of 12 samples distributed on 4 lanes of the flow cell. Reads were demultiplexed and aligned using Burrows-Wheeler Aligner (BWA) software<sup>39</sup> to human reference genome 19. Insertion-deletion realignment was performed as well as recalibration based on Genome Analysis Toolkit (GATK)<sup>40</sup> quality scores. To call single-nucleotide variants (SNVs) and deletions-insertions variants (DIVs),

UnifiedGenotyper and GATK Variant quality score recalibration were performed as described previously<sup>41</sup> with minor modifications. Generated lists of SNVs and DIVs were annotated with ANNOVAR<sup>42</sup> using dbSNP Build 137. Variants present in 1000 Genomes Project data (in February 2012) and/or dbSNP Build 137 with minor allele frequency of  $\geq 0.01$  were excluded from further analyses; lists were filtered to include only nonsense, missense and splice-site variants present in the shared homozygous region on chromosome 3 at 9.52–11.04 Mb.

**Sequence analysis.** We used SIFT<sup>43</sup>, PolyPhen-2 (ref. 44) and ConSurf<sup>45</sup> to analyze the effects of amino acid substitutions on *JAGN1* (**Supplementary Table 3**). We gathered sequences for homologs to *JAGN1* ([NP\\_115881.3](#)) by running three rounds of PSI-BLAST<sup>46</sup> with default settings against the NCBI non-redundant database current as of 12 January 2009. We kept only sequences that aligned with an  $E$  value of at most  $1 \times 10^{-4}$  after three rounds of PSI-BLAST. We eliminated sequences that aligned with more than 90% identity with human *JAGN1* or with each other, retaining a total of 41 homologs, including human *JAGN1*. We created a multiple alignment using ClustalW 1.83 (ref. 47) with default settings. We ran SIFT<sup>43</sup>, ConSurf<sup>45</sup> and PolyPhen-2 (ref. 44) on 14 February 2013, using web interfaces. For SIFT and ConSurf, we provided the alignment produced by ClustalW.

**Immunoblot analyses.** Immunoblotting for the expression levels of BIP and GAPDH was performed as described previously<sup>5</sup>. Total protein was extracted from EBV-immortalized B cell lines and primary fibroblasts from the affected subjects and controls. The primary antibodies used to detect *JAGN1* were derived from peptides in the mouse sequence ([NP\\_080641](#)). Polyclonal rabbit antibodies to *JAGN1* were raised in a rabbit and were affinity purified against the keyhole limpet hemocyanin (KLH)-coupled peptide ASRAGPRAAGTDGSDFFQHR (positions 2–20 of [NP\\_080641](#)) (1:500 dilution). Monoclonal mouse antibody to GAPDH (1:1,000 dilution; Santa Cruz Biotechnology, sc-32233) was used as a loading control.

**Electron microscopy.** Sample preparation for transmission electron microscopy was performed as described previously<sup>5</sup>. Samples were assessed using a Philips electron microscope 301 (Fei).

**Apoptosis assays.** Neutrophil granulocytes were isolated from peripheral blood and exposed to staurosporine (2.5  $\mu\text{g/ml}$ ; Sigma-Aldrich) to induce apoptosis. Neutrophils were isolated from a healthy donor 1 d after an injection with rhG-CSF. Cells were stained with Annexin V (Life Technologies) and propidium iodide (Sigma-Aldrich) and analyzed by flow cytometry, similarly to previous studies<sup>5</sup>. Flow cytometry data were analyzed using FlowJo version 9.0.1.

**Measurement of mitochondrial membrane potential in neutrophil granulocytes.** Neutrophil granulocytes were treated with valinomycin (Sigma-Aldrich), a potassium-specific transporter leading to the dissipation of mitochondrial membrane potential ( $\Delta\psi_{\text{mt}}$ ). Flow cytometry using the lipophilic cation JC-1 (Life Technologies) was performed as described previously<sup>6</sup> to measure the relative percentage of cells with low  $\Delta\psi_{\text{mt}}$  values.

**Cloning of *JAGN1*.** Two fusion constructs were generated: *EGFP* was cloned upstream (*EGFP-JAGN1*) or downstream (*JAGN1-EGFP*) of human *JAGN1*. The full-length *JAGN1* ORF was amplified from cDNA. The PCR primers for *EGFP-JAGN1* contained a BglII or SalI restriction site (**Supplementary Table 5**). The PCR primers for *JAGN1-EGFP* contained an NheI or BamHI restriction site (**Supplementary Table 5**). Both PCR products were subcloned into the pGEM-T Vector System I (Promega). The BglII and SalI digestion sites were used for insertion into pEGFP-C1 plasmid (Clontech Laboratories) to create *EGFP-JAGN1*. The NheI and BamHI digestion sites and the pEGFP-N1 plasmid (Clontech Laboratories) were used to create *JAGN1-EGFP*. The Kozak consensus sequence was integrated upstream of the start codon of *JAGN1-EGFP*. The sequences of the constructs were verified by digestion and sequencing. Vectors from Clontech Laboratories were provided by A. Schambach (Hannover Medical School).

**Cell culture.** Cells were cultured at 37 °C in a humidified atmosphere with 5% CO<sub>2</sub> in glucose-rich DMEM (PAA) containing 10% FCS (Life Technologies, Gibco) for HeLa cells (tested negative for mycoplasma contamination) or 20% FCS for fibroblasts and 50 units/ml penicillin, 50 µg/ml streptomycin and 292 µg/ml L-glutamine (all from Gibco).

**Immunofluorescence-based studies to assess JAGN1 intracellular localization.** To generate **Figure 3a**, HeLa cells were seeded onto glass coverslips (Thermo Fisher Scientific) and cultured for at least 24 h. After washing with PBS, cells were fixed in 3.7% paraformaldehyde for 35 min and permeabilized with PBS containing 0.1% Triton X-100. Cells were blocked with PBS containing 5% BSA at room temperature for 40 min and subsequently incubated with polyclonal rabbit antibody to JAGN1 and a mouse monoclonal antibody to human calnexin (BD, 610523; 1:100 dilution) for 1 h. Cells were then washed in PBS and incubated for 1 h with either Alexa Fluor 488–conjugated goat anti-rabbit IgG or Alexa Fluor 594–conjugated goat anti-mouse IgG secondary antibody (Life Technologies). Nuclei were stained with DAPI for 15 min at room temperature. Coverslips were mounted in Fluorescent Mounting Medium (Dako). Images were acquired with an Olympus FV1000 confocal laser scanning microscope using a 63× objective and analyzed with ImageJ<sup>48</sup>.

To generate the data in **Supplementary Figure 14**, HeLa cells and fibroblasts were cultured on coverslips (Thermo Fisher Scientific). After 24–36 h, transient transfection was performed with Lipofectamine 2000 (Life Technologies) according to the manufacturer's instructions. HeLa cells and fibroblasts were transfected with *JAGN1-EGFP* or *EGFP-JAGN1* construct. After 36–48 h, cells were fixed with 4% paraformaldehyde in PBS for 25 min and then permeabilized with 0.2% saponin in PBS for 5 min. All the following steps were performed with 0.5% saponin. After quenching with 50 mM NH<sub>4</sub>Cl in PBS for 10 min, we blocked nonspecific binding sites by incubating with 10% goat serum in PBS for 30 min. To stain the ER, we used mouse monoclonal antibody to calnexin (1.25 µg/ml; BD, 610523), and, to stain the Golgi apparatus, we used mouse monoclonal antibody to golgin-97 (1:200 dilution; Molecular Probes, Life Technologies, A-2127). Alexa Fluor 555–conjugated goat anti-mouse IgG (1:1,000 dilution; Molecular Probes, Life Technologies, A21424) was used as a secondary antibody. For nuclear staining, cells were stained with Hoechst (33342, Molecular Probes, Life Technologies), and coverslips were mounted in Fluorescence Mounting Medium (Dako). Between all steps, coverslips were washed with PBS. Mitochondria staining was performed with MitoTracker Red CMXRos (150 nm; 30 min; Molecular Probes, Life Technologies), according to the manufacturer's instructions. Images were acquired with a Leica DM IRB inverted confocal microscope (Leica Microsystems) equipped with a TCS SP2 AOBs scanning head and analyzed using the Leica software LCS and ImageJ software.

**Processing of neutrophils to obtain N- and O-glycans for subsequent glycomic analysis.** For glycomics experiments, each human sample (~3 million cells) was subjected to sonication in the presence of detergent (CHAPS) and treated as described previously<sup>49</sup>.

**Mass spectrometric N- and O-glycomic analyses.** Permethylated N- and O-glycans prepared as described above were analyzed on a 4800 MALDI-TOF/TOF mass spectrometer (Applied Biosystems, Life Technologies), as described previously<sup>21</sup>.

**Gaussia luciferase secretion assays.** To perform *Gaussia* luciferase secretion assays, HeLa cells were first seeded on 6-well plates 1 d before transfection. To silence *JAGN1*, cells were transfected with either negative control siRNA (4404021) or *JAGN1* siRNAs 1 and 2 (s39100 and s39101, respectively, Life Technologies) using the Lipofectamine RNAiMax kit (Life Technologies) according to the manufacturer's instructions. Medium was changed the following day. On day 4, cells were transfected with pCMV-Gluc (New England BioLabs) using JetPEI transfection reagent (PolyPlus Transfection). Medium was replaced on the following morning, and cells were either treated with thapsigargin (1 µg/ml; AppliChem) or left untreated. Samples were collected 8 h after the change of medium. Luciferase activity was measured using coelenterazine as a substrate (Biolum *Gaussia* Luciferase Assay Kit, New England BioLabs). Results are given as the ratio between samples averaged over three independent experiments.

To verify knockdown of *JAGN1*, cells were lysed with buffer containing 20 mM Tris-HCl, pH 7.4, 150 mM NaCl, 1 mM EDTA, 1 mM EGTA, 5 mM NaF, 1 mM orthovanadate, 10% glycerol, 1% Triton X-100, 0.5% NP-40 and protease inhibitors before samples were used for protein blot analysis. The knockdown of *JAGN1* was detected using an antibody to JAGN1 (see above), and actin (1:1,000 dilution; sc-47778, Santa Cruz Biotechnology) was used as a loading control.

**Tandem affinity purification and mass spectrometry.** Human *JAGN1* cDNA was cloned into C- and N-terminal pTO-STREP-HA-GW vectors (Life Technologies). The plasmids were transfected into HEK293 FLP-In-TREx cells (Life Technologies), to express JAGN1 protein upon administration of doxycycline. Generation of JAGN1 HEK293 FLP-In TREx cells and subsequent tandem affinity purification coupled to mass spectrometry (TAP-MS) were performed as described previously<sup>50</sup>.

Five confluent 15 cm dishes were stimulated with 1 µg/mL doxycycline (Thermo Fisher Scientific) for 24 h. Cells were harvested and lysed in TNN-HS buffer (50 mM HEPES pH 8.0, 150 mM NaCl, 5 mM EDTA, 0.5% NP-40, 50 mM NaF, 1 mM Na<sub>3</sub>VO<sub>4</sub>, protease inhibitors from Sigma-Aldrich). STREP-HA-JAGN1 was purified using strepTactin Sepharose beads (IBA, Goettingen, Germany) followed by elution with biotin (Alfa Aesar, Karlsruhe, Germany). The biotin eluate was then immunopurified with anti-HA-agarose beads (Sigma-Aldrich). The bound material was eluted with 100 mM formic acid (Suprapur, Merck Millipore, Darmstadt, Germany) and neutralized with triethylammonium bicarbonate (TEAB) (Sigma-Aldrich). The samples were digested with trypsin (Promega) and 2 × 5% v/v of the resultant peptides were analyzed by LC-MS/MS on a linear trap quadrupole (LTQ) Orbitrap Velos mass spectrometer (Thermo Fisher Scientific) coupled to an 1200 series high-performance liquid chromatography system (Agilent Technologies, Santa Clara, CA, USA)<sup>24</sup>.

The acquired raw MS data files were converted into MASCOT generic format (mgf) files, and the resultant peak lists were queried against the human SwissProt database (v.2010.09) using the search engines MASCOT (v2.3.02, MatrixScience, London, UK) and Phenyx (v2.6, GeneBio, Geneva, Switzerland)<sup>51</sup>. One missed tryptic cleavage site was allowed. Carbamidomethyl cysteine was set as a fixed modification, and oxidized methionine was set as a variable modification. The peptides which were independently identified by the two algorithms were combined by discarding all the spectra identifying different peptides, and grouping the remaining spectra into protein groups sharing peptides. The peptide score thresholds of both search engines were set such that the combined results achieved a protein group false detection rate (FDR) of <1%, as determined by applying the whole procedure against a reversed database. This resulted in imposing a Phenyx z-score >4.75 for single peptide identifications or >4.2 for multiple peptide identifications, and Mascot single peptide identifications ion score >40, multiple peptide identifications ion score >14. Individual peptides selected by this procedure featured a false positive rate of <0.1%.

In parallel, TAP-MS of N- and C-terminal STREP-HA-GFP FLP-In-TREx cells were performed. All proteins identified from the STREP-HA-GFP experiments were removed from the JAGN-1 interactors list. The final JAGN1 interaction network was drawn using Cytoscape (version 2.8.1).

**Immunoprecipitation assay.** For the immunoprecipitation assay, JAGN1 HEK293 FLP-In TREx cell lines expressing N- and C-terminally tagged versions of JAGN1 were used. Doxycycline stimulation and lysate isolation were performed as for the tandem affinity purification, and 10% of the input material was used. The lysates were precleared with Protein G-Sepharose beads (GE Healthcare) and immunopurified with anti-HA agarose beads (Sigma-Aldrich). Input and immunoprecipitation samples were separated by SDS-PAGE, blotted and stained with antibodies against COPA (Sigma-Aldrich; 1:1,000 dilution), COB2 (Sigma-Aldrich; 1:1,000 dilution), GAPDH (Santa Cruz Biotechnology) and HA tag (Sigma-Aldrich; 1:4,000 dilution).

**G-CSF-R studies in neutrophil granulocytes from a healthy donor and affected subjects.** Granulocytes were isolated from the peripheral blood of a healthy donor and three affected subjects from distinct families A (P2), G (P12) and H (P13) using density gradient centrifugation (Ficoll-Histopaque, Amersham Biosciences). Cells were lysed as described in "*Gaussia* luciferase

secretion assays,” and the sample for the healthy donor was either left untreated or treated with PNGase F (New England BioLabs) according to the manufacturer’s instructions. G-CSF-R was detected in protein blotting using an antibody from Santa Cruz Biotechnology (H-176, sc-9173; 1:250 dilution). Actin (Santa Cruz Biotechnology) was used as a loading control.

**G-CSF stimulation assays in HeLa cells.** HeLa cells were seeded on 6-well plate and were transfected 1 d later with *JAGN1*-specific siRNA oligonucleotides. On day 4, cells were transfected with wild-type *CSF3R-GFP* construct in the pMMP vector using JetPEI (PolyPlus Transfection) according to the manufacturer’s instructions. The day after transfection, starvation was started, using medium containing 0.5% serum. The following day, cells were stimulated with 100 ng/ml G-CSF (Amgen) for the indicated times, and cells were lysed as described in “*Gaussia* luciferase secretion assays.” Phosphorylated STAT3 (Tyr705, Cell Signaling Technology, 9131; 1:1,000 dilution), total STAT3 (BD Biosciences, 610190; 1:1,000 dilution), G-CSF-R (Santa Cruz Biotechnology, H-176, sc-9173; 1:250 dilution) and *JAGN1* (N terminus; 1:1,000 dilution) were detected by protein blotting. Actin (Santa Cruz Biotechnology, sc-47778, 1:1,000 dilution) was used as a loading control.

**Immunofluorescent and glycosylation studies of G-CSF-R and neutrophil elastase in *JAGN1*-silenced HeLa cells.** HeLa cells were seeded on coverslips in 6-well plates and were transfected using reverse transfection with control siRNA or *JAGN1*-specific siRNA 1 or 2 using the Lipofectamine RNAiMax kit (Life Technologies). Medium was changed the following day. Two days after transfection with siRNA, cells were again transfected using JetPEI transfection reagent (PolyPlus Transfection) with construct for either HA-tagged wild-type ELANE in the pLPCX-vector (Clontech Laboratories) or wild-type G-CSF-R-GFP in the pMMP vector. Cells were fixed with 4% paraformaldehyde 36–48 h later and were stained following the first immunofluorescence staining protocol described above. The primary antibodies used were polyclonal goat antibody to neutrophil elastase (Santa Cruz Biotechnology, C-17; 1:100 dilution) and rabbit antibody to G-CSF-R (Santa Cruz Biotechnology, H-176; 1:100 dilution). The secondary antibodies used were Alexa Fluor 488-conjugated donkey anti-goat IgG and Alexa Fluor 594-conjugated goat anti-rabbit IgG. Images were acquired with an Olympus FV1000 confocal laser scanning microscope and a 63× objective.

For glycosylation studies, cells were lysed as described in “*Gaussia* luciferase secretion assays” 36–48 h after transfection with plasmid and cleared protein lysate was either left untreated or treated with EndoH or PNGase F

(New England BioLabs) according to the manufacturer’s protocol. Samples were subjected to protein blot analysis. The primary antibodies used were rabbit antibody to the N terminus of *JAGN1* (1:1,000 dilution), rabbit antibody to G-CSF-R (Santa Cruz Biotechnology, H-176; 1:250 dilution) and rabbit antibody to neutrophil elastase (Santa Cruz Biotechnology, C-17; 1:1,000 dilution). Actin (Santa Cruz Biotechnology; 1:1,000 dilution) was used as a loading control.

35. Pfeifer, D. *et al.* The hyper-IgE syndrome is not caused by a microdeletion syndrome. *Immunogenetics* **59**, 913–926 (2007).
36. Fishelson, M. & Geiger, D. Exact genetic linkage computations for general pedigrees. *Bioinformatics* **18**Suppl 1, S189–S198 (2002).
37. Hamada, T. *et al.* Lipoid proteinosis maps to 1q21 and is caused by mutations in the extracellular matrix protein 1 gene (*ECM1*). *Hum. Mol. Genet.* **11**, 833–840 (2002).
38. International HapMap Consortium. A second generation human haplotype map of over 3.1 million SNPs. *Nature* **449**, 851–861 (2007).
39. Li, H. & Durbin, R. Fast and accurate long-read alignment with Burrows-Wheeler transform. *Bioinformatics* **26**, 589–595 (2010).
40. DePristo, M.A. *et al.* A framework for variation discovery and genotyping using next-generation DNA sequencing data. *Nat. Genet.* **43**, 491–498 (2011).
41. Salzer, E. *et al.* Combined immunodeficiency with life-threatening EBV-associated lymphoproliferative disorder in patients lacking functional CD27. *Haematologica* **98**, 473–478 (2013).
42. Wang, K., Li, M. & Hakonarson, H. ANNOVAR: functional annotation of genetic variants from high-throughput sequencing data. *Nucleic Acids Res.* **38**, e164 (2010).
43. Ng, P.C. & Henikoff, S. Accounting for human polymorphisms predicted to affect protein function. *Genome Res.* **12**, 436–446 (2002).
44. Adzhubei, I.A. *et al.* A method and server for predicting damaging missense mutations. *Nat. Methods* **7**, 248–249 (2010).
45. Ashkenazy, H., Erez, E., Martz, E., Pupko, T. & Ben-Tal, N. ConSurf 2010: calculating evolutionary conservation in sequence and structure of proteins and nucleic acids. *Nucleic Acids Res.* **38**, W529–W533 (2010).
46. Altschul, S.F. *et al.* Gapped BLAST and PSI-BLAST: a new generation of protein database search programs. *Nucleic Acids Res.* **25**, 3389–3402 (1997).
47. Larkin, M.A. *et al.* Clustal W and Clustal X version 2.0. *Bioinformatics* **23**, 2947–2948 (2007).
48. Girish, V. & Vijayalakshmi, A. Affordable image analysis using NIH Image/ImageJ. *Indian J. Cancer* **41**, 47 (2004).
49. Jang-Lee, J. *et al.* Glycomic profiling of cells and tissues by mass spectrometry: fingerprinting and sequencing methodologies. *Methods Enzymol.* **415**, 59–86 (2006).
50. Pichlmair, A. *et al.* Viral immune modulators perturb the human molecular network by common and unique strategies. *Nature* **487**, 486–490 (2012).
51. Colinge, J., Masselot, A., Giron, M., Dessingy, T. & Magnin, J. OLAV: towards high-throughput tandem mass spectrometry data identification. *Proteomics* **3**, 1454–1463 (2003).